P3A Final Report
Multi-scale tests of gravity

KHALLOUF Elias, MAGNAN Nathan

March 2020

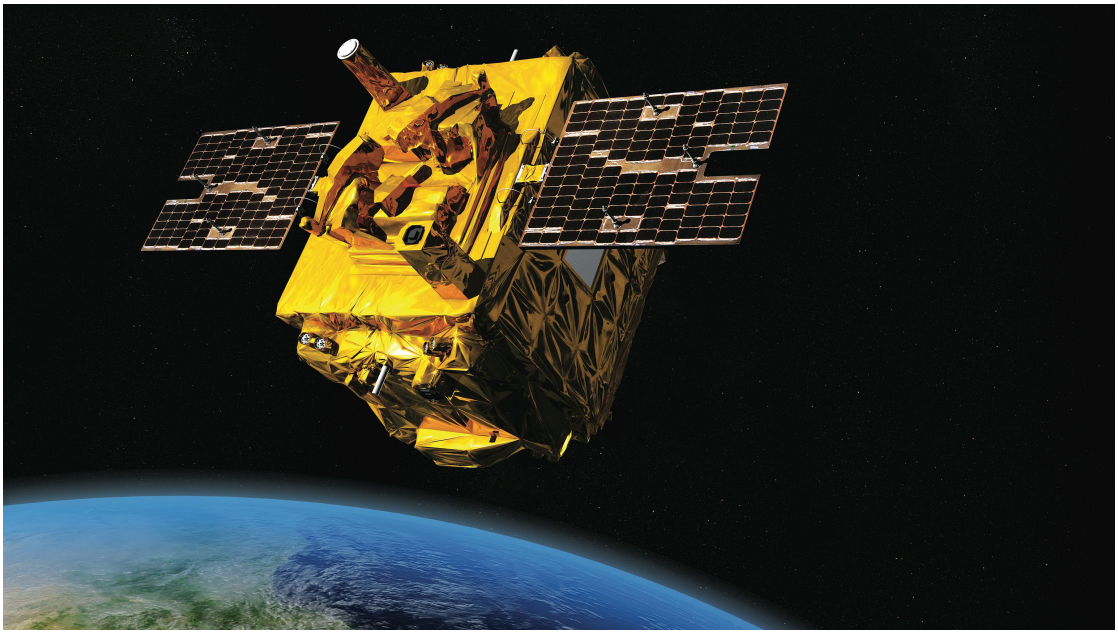

Contents

Introduction

Gravity is one of the most important phenomena in cosmology and astrophysics. Yet, it is the least well understood fundamental force, with general relativity failing to explain some observations at the galactic scale [2][4] unless we add dark matter and dark energy.

In particular, there is a myriad of different models to explain this force and its deviations to general relativity : from the introduction of non-standard particles such as the weakly interacting massive particle [6] or the chameleon particle [10], to modified Newtonian dynamics [9]. All of these theories are designed to explain the observations that differ from the predictions of general relativity. But no other prediction from any of these theories has yet been confirmed or refuted by experience.

The proposed Voyage 2050 mission would be a new experiment with hopefully the precision needed to refute some of the models. The method would be to launch a probe to the outer solar system and monitor its trajectory to eliminate the models that predicted a significantly different trajectory.

There are several major obstacles to overcome. First, the distribution of mass in the solar system is not well known, especially in the Kuiper belt. Hence the trajectory expected by each of the models comes with uncertainties. Second, there are other forces that are non gravitational, such as solar radiation pressure, solar winds, or thermal forces. Hence the trajectory observed needs to be corrected from these effects before it can be analyzed.

This is done thanks to an unbiased electrostatic accelerometer developed at ONERA. Since an accelerometer cannot detect gravitational accelerations, it will measure all non gravitational accelerations. That of ONERA yields a precision of 10^{-12} ms^{-2}. The purely gravitational trajectory can then be deduced by subtracting the non-gravitational accelerations from the observed movement.

During this P3A, we first design a model for the trajectory of objects in the outer solar system, under different gravitational models. We then use this model to quantify the ability of ONERA's accelerometer to discriminate between the standard model of gravitation and other models from the literature, especially the tensor-vector-scalar theory of gravity [9].

Acknowledgments

First and foremost, we wish to thank deeply our tutor M. Joel BERGE, for offering us to do research on this very interesting subject that is non-Newtonian gravity, for guiding us through numerous technical obstacles, and also for taking the time to find us an internship tutor at the JPL. Although, sadly, neither of us could use that opportunity.

We would also like to express our gratitude to M. Pascal CHABERT for all the time he took this year for the students of the PA : the classes on plasma physics, the master-classes, the trip to the CNES, and the help on finding research internships and choosing a 4A.

We would finally like to thank M. Michel FERRERO for showing us how to do par-ralelized multi-processing on Python. And we would like to thank ONERA both at Chatillon and at Palaiseau for hosting us half a day a week.

1 Scientific objectives of the proposed Voyage 2050 mission, and scope of the P3A

In general relativity, gravity is equivalent to the curvature of space-time. And the geometry of space-time is linked to the distribution of matter and energy by Einstein Field Equations (EFE) [1] :

$$G_{\mu\nu} = \frac{8\pi G}{c^4} T_{\mu\nu}$$

$$G_{\mu\nu} = R_{\mu\nu} - \frac{1}{2} R g_{\mu\nu}$$

$G_{\mu\nu}$ is Einstein's tensor. It is linked by the first equation to the energy-impulsion tensor $T_{\mu\nu}$ that represents the distribution of matter. $G_{\mu\nu}$ is also linked to the geometry of space-time by the second equation, with $R_{\mu\nu}$ being Ricci's curvature tensor and $g_{\mu\nu}$ the metric.

This equation is the part of general relativity that generalize Newton's law of gravitation. It explains incredibly well several observations such as the period of Mercury's orbit, gravitational lensing or gravitational waves. Yet there are observational limits to this theory:

- H. Van de Hulst and M. Schmidt observed in 1957 that the M31 rotation curve (that is, the curve of the average radial velocity of the stars in galaxy M31, depending of distance to the center of the galaxy) does not match the curve that would be predicted from the mass distribution that is observed in M31. This observation has been reproduced for several other galaxies since then [2].

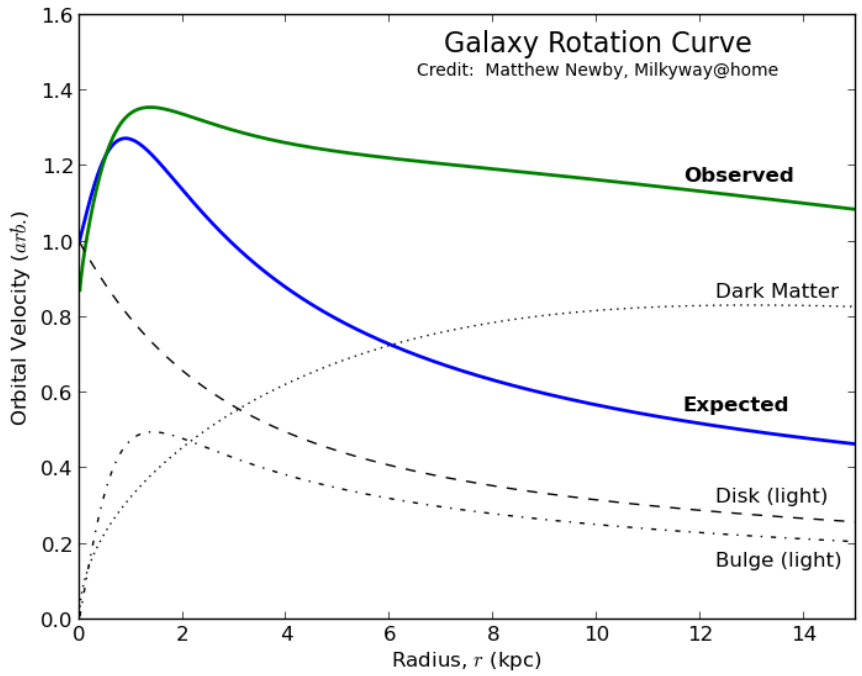

Figure 1: Rotation curve observed vs. expected from the observed mass distribution [3]

- F. Zwicky used in 1933 the virial theorem to calculate the total mass of the galaxies in the Coma cluster, and observed a large discrepancy with the mass expected from the light received during observations [4].

To explain this observational limits to general relativity, we know of 2 approaches:

- The first solution is to modify the right-hand side of the first EFE, that is to modify $T_{\mu\nu}$ and the distribution of matter in the universe. This is done by introducing a dark matter that would be a massive matter that does not interact with electromagnetic radiation [5]. To obtain the observed abundance of such particles via thermal production, a specific value for the self-annihilation cross-section of those particles is needed: $\langle \sigma v \rangle = 3\ 10^{-26}\ \mathrm{cm}^3\ \mathrm{s}^{-1}$ [6]. A very good candidate used to be the Weakly Interacting Massive Particle (WIMP) that had been already been predicted by super-symmetric extensions of the standard model. But those super-symmetric theories have been found not to match observations at LHC.
  This first approach also includes the introduction of dark energy, an unknown form of energy that would explain the universe's expansion rate [7]. On the whole, across the entire universe, the energy distribution presented in figure 2 is expected:

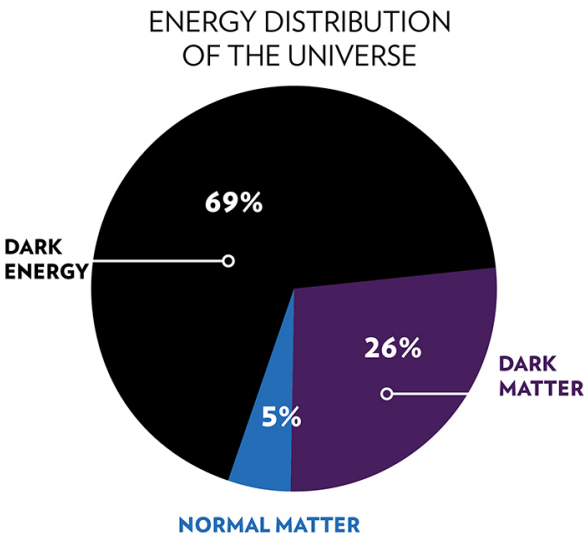

Figure 2: Expected distribution of total energy of the universe into baryonic matter, dark matter, and dark energy [8]

- The second approach is to modify the definition of $G_{\mu\nu}$, that is to modify the right-hand side of the second EFE. The MOdified Newtonian Dynamics (MOND) theory can be generalized to be coherent with special relativity through the tensor-vector-scalar gravity theory [9], which also englobes Brans & Dicke theory. In this TVS theory, a Yukawa potential is added to Newton's gravitational potential :

$$V(r) = -\frac{GM_AM_B}{r}(1 + \alpha e^{-r/\lambda})$$

  Since Newton's potential makes excellent prediction at the scale of the solar system, this theory is often coupled with a theory that explains a screening effect that

makes parameters α and λ very weak in stellar systems but noticeable on the galactic scale. On such theory is the Chameleon Particle theory [10]. Notably, this theory is also a theory for Dark Energy. The 2 approaches are not incompatible.

The objective of the Voyage 2050 mission would be to reach the outer solar system and, once there, to measure the force of gravity to deduce information either on the distribution of dark matter in the solar system, or on the acceptable values for α and μ. There has already been such studies at different scales, whose results are given in figure 3. But they could not find non-zero values for the parameters and only could exclude some values:

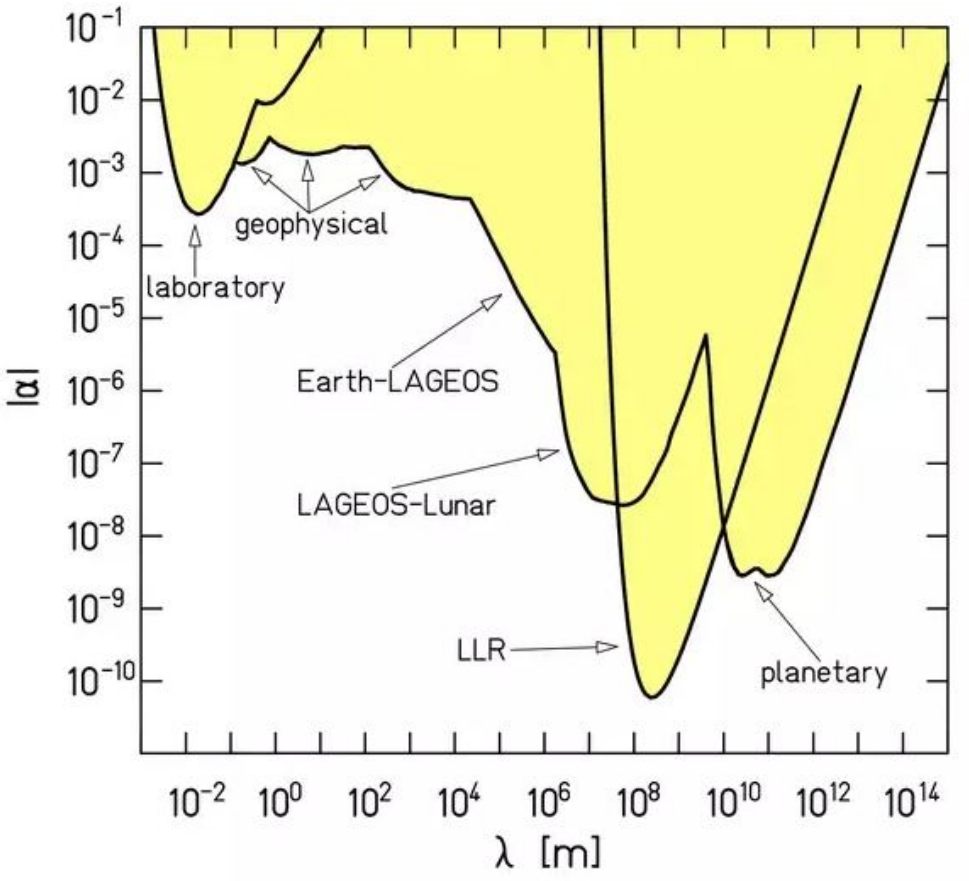

Figure 3: α - λ couple exclusion area [11]

The inertial mass and the gravitational mass are equal to each other [12]. Hence the acceleration $\vec{a}$ and the gravitational field $\vec{g}$ are equal for an ideal mass. Since an accelerometer measures the change in distance between a cage and a test mass, and since both the test mass and the cage feel the same gravitational field, an accelerometer cannot measures gravitational accelerations.

Hence, Voyage 2050's solution to measure the gravitational force is to send a probe in the outer solar system, to measure its position thanks to a radar and its non-gravitational accelerations thanks to an accelerometer. With that data, one can compute the position the probe would have had without any non-gravitational acceleration. And then deduce the equations for gravitation from the corrected trajectory of the probe.

This P3A is a preliminary study whose goal is to find how much information one can expect to gain from the mission. If we had perfect knowledge of the corrected trajectory, we would deduce perfectly the law of gravitation by a double derivation. But the accelerometer, the radar, and the numerical integration of the law of gravitation all produce uncertainties. With that in mind, how much will we be able to restrain the set of acceptable values for α and μ ?

To answer this question, we have to model numerically the trajectory of the probe in Newton's potential and in Yukawa's potential. Then we have to find a quantity that gives, for two given trajectories with uncertainties, the statistical significance of the differences between these trajectories. Then, we must compute this quantity over a grid $(\alpha,\ \lambda)$ to find the set of values of these parameters for which we will been able to discriminate between a Newtonian trajectory and a Yukawa trajectory.

Additionally, we can model numerically the non-gravitational accelerations that will be measured during the mission. Because it allows to research the ability of the mission to provide more information on the outer solar system environment. And it makes sure there will not be any non-linear effects such as saturation of the accelerometer.

2 Modeling the outer solar system environment

Our first goal is to simulate the trajectory of a probe in the usual Newtonian gravitational potential, but also in Yukawa's potential. These potentials dominate the large-scale shape of the trajectory, but there are also many perturbations that have to be taken into account in order to obtain a precise trajectory. In this section, we describe these effects and the models we use to simulate them in the outer solar system.

2.1 Gravitational accelerations

As introduced in the *Principia Mathematica*, the Newtonian model of gravity is characterised by a force in r^{-2}. The force exerted by a body A on a body B is:

$$\vec{F_{A/B}} = -\frac{GM_AM_B}{r_{AB}^2}\hat{r_{AB}}$$

By defining $\mu = GM_A$ we get the acceleration of the Newtonian gravitational force:

$$\vec{a} = -\frac{\mu}{r_{AB}^2}\hat{r_{AB}}$$

Yukawa's model of gravity is named as such because it is based on the addition of a Yukawa potential to the Newtonian potential [11]. This potential is characterised by an additional exponential decay defined using two parameters, α and λ. And since Yukawa's model is seen as a correction of Newton's, α is very small:

$$V(r) = -\frac{GM_AM_B}{r_{AB}} \times (1 + \alpha e^{-\frac{r_{AB}}{\lambda}})$$

Taking the gradient of this potential and using the earlier definition of μ, we get an acceleration given by:

$$\vec{a} = -\frac{\mu}{r_{AB}^2} \times (1 + \alpha e^{-\frac{r}{\lambda}}(1 + \frac{r_{AB}}{\lambda}))\hat{r_{AB}}$$

2.2 Force exerted by the Kuiper belt

Although this force is gravitational, it necessitates a specific consideration because the precedent subsection considers only point masses. But the Kuiper belt extends radially over several astronomical units : even on the solar system scale it cannot be considered punctual. We considered 3 options to model the belt's influence :

- We could consider the belt as a clumpy torus and do a simulation with N bodies with N large. This approach is used in [13] but would be very slow in our case because it implies computing N forces at each time step.
- We could consider the belt as a torus with a simple enough density distribution, and compute the force as the integral of the force exerted by point masses over the torus. But this approach would necessitate a rather heavy numerical integration at each time step, which is also quite slow.

- We could consider the belt as a torus with circular cross-section and homogeneous density. Under those hypotheses, we find in [14] a semi-analytic formula for the Newtonian potential far from the torus, using the complete elliptical integrals of the first and second kinds [15]. Since there are simple differential relations between this K and E, it is quite easy to find the force exerted from the potential by taking the gradient.

We chose the third option because it is the fastest algorithmically and its hypotheses are reasonable in our study : the probe will be very far from the belt so the Taylor expansion is justified. And the belt mass is very low (about two percent of Earth's mass) so approximations on its geometry and density distribution will have a very weak impact on the probe's simulated trajectory.

The expression we found for the force is too long to be written here, but the math is given in Appendix A. Since this method was developed for a Newtonian potential, we also give in Appendix A our work to adapt it.

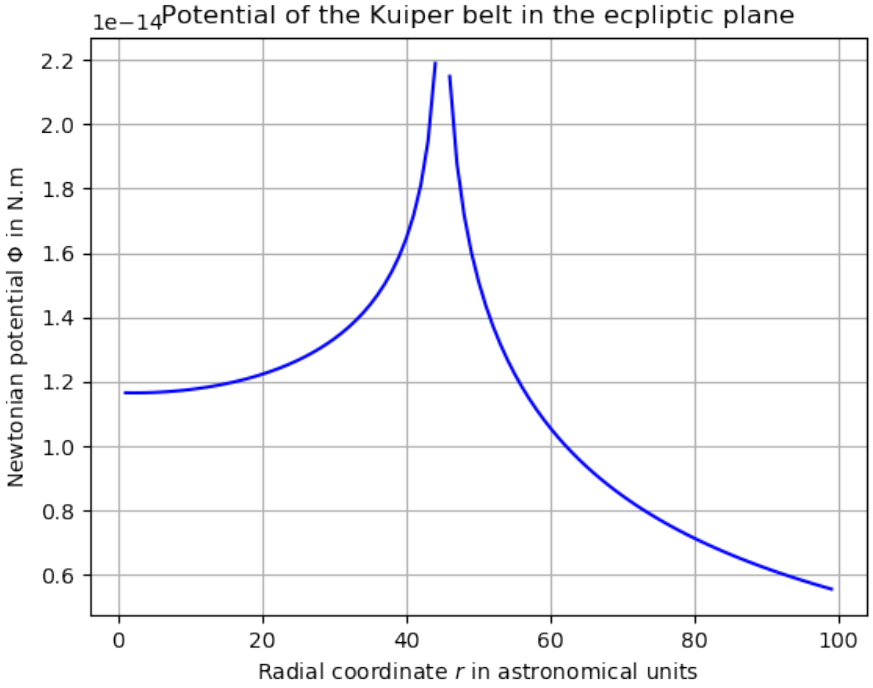

Figure 4: Approximated Newtonian potential of the Kuiper belt in the ecliptic plane, as a function of the radius. We can see that the center of the belt ($r = 0$) is an unstable equilibrium. We can also see that the belt is attractive on its outside, with a potential in $1/r$. This is coherent with physics.

2.3 Solar radiations

The sun emits a large number of photons which transmit linear momentum to the probe via absorption and reflection on its surface. Thus a force is exerted on the probe,

impacting its trajectory. The impulse of a single photon is given by:

$$P_\nu = \frac{E_\nu}{c}$$

By defining $\phi = \frac{dE}{dt \times dA}$ the flux of energy through a surface dA, we get that the impulse of the photon flow at the satellite's position:

$$dI = \frac{\Delta p}{\Delta t} = \frac{\phi}{c} dA$$

Given that the solar flux amounts to $\phi = 1367$ W.m^{-2} at a distance of 1AU and is isotropic, we can get the impulse of the photon flow at any distance needed trough an inverse square law. To find the force exerted on the satellite, we now have to take into account the orientation of the satellite's surface and its absorption rate (see figure 5).

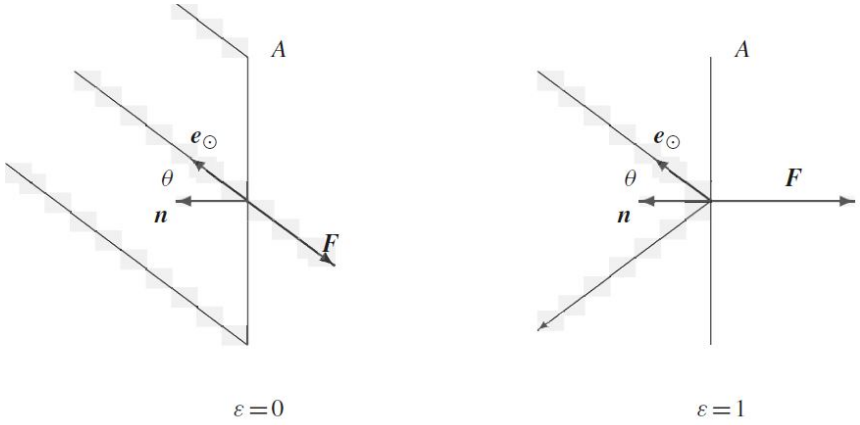

Figure 5: A photon that is reflected transmits twice the momentum in the direction normal to the surface [16]

Taking this effect into account, we get for an absorption rate of $1 - \epsilon$ (ϵ being the reflectivity of the surface) the following force :

$$d\vec{F_{gen}} = -dI \cos\theta \times ((1-\epsilon)\hat{e_\theta} + 2\epsilon \cos\theta \hat{e_n})$$

Finally, by integrating this force on our spherical satellite model, we get:

$$\vec{F_{real}} = (1+\epsilon)\pi r^2 \frac{\phi}{c} \hat{e_r}$$

2.4 Solar winds

The solar wind is a stream of charged particles released from the upper atmosphere of the sun. This stream is mainly composed of electrons, protons and alpha particles, with traces of other heavy ions. This wind exits isotropicaly, creating the heliosphere. We can distinguish two types of solar winds depending on their velocity [17]:

- The slow solar wind with a speed of 300-500 km/s in the near-earth space.
- The fast solar wind with a typical speed of 750 km/s in the near-earth space but with a lower density.

This flow of high speed particles exerts a pressure on any object it encounters proportional to the relative speed and the density of the jet. The pressure is given by $P = m_p \times n \times V^2$ where P is the pressure, m_p the mass of a proton, n the density of protons, and V the velocity of the protons.

This pressure can greatly affect the trajectories of satellites, especially close to the sun where the velocity is the highest. Further from the star, this wind will decelerate, supposedly creating a termination shock where the heliosphere ends, at around 84 AU from the sun [18][19].

The force applied on a spherical probe of radius r from the solar wind is given by [19]:

$$\vec{F} = 2\pi r^2 \times d_{sun}^2 \times \phi \hat{e_r}$$

Where d_{sun} is the distance from the Sun to the probe, and ϕ is the flux of mass:

$$\phi = m_p \times V \times \frac{n_0}{4\pi r_{sun}^2}$$

m_p is the mass of protons, V the relative velocity of the solar wind to the satellite, n_0 the number of protons ejected by the sun per second and r_{sun} the radius of the sun.

2.5 Thermal force

The probe can be considered as a black body. Once heated such a body emits radiations proportional to its temperature. As before, the radiations emitted have an impulse equals to:

$$P_\nu = \frac{E_\nu}{c}$$

Thus this radiation will generate a force on the satellite, this is what caused Pioneer's drift [20]. In an ideal case, the temperature of the satellite would be homogeneous, leading to isotropic emission hence no force. However in reality neither internal heating nor exposition to the sun is the same for all surfaces of the probe, resulting in faces warmer than other. Those faces will emit more radiations, hence generating more recoil. This will cause the satellite to undergo a non-zero thermal recoil force.

We expect that the surface exposed to the sun will be the warmest, thus the propulsion would be a radial propulsion from the sun towards outer space. However, in case the satellite rotates, we will observe a Yarkovsky effect where the side that was just exposed to the sun is hotter than the side that is currently exposed, thus generating angular propulsion as well.

2.6 Interstellar dust

Interstellar space is filled with dust. Even though the density of the dust is very low, it still affects the mechanical energy of a satellite, and reduces its speed. A crude model is that of a drag:

$$F = c \times nm \times v^2$$

If we assume a drag coefficient $c = 1$, a dust density of $n = 10^{-6}$ part./m^3, an average mass $m = 10^{-17}$ g for the dust particle and a stationary dust ($v = v_{sat}$) [21], we find a force 9 orders of magnitude below that of gravity. Hence we considered this effect to be negligible and we did not model it.

3 Computational aspects of trajectory modelling

A large part of our work has been to develop a Python library with the functions necessary to compute the trajectory of a probe in the outer solar system, with the numerical precision required by the P3A's objectives, and taking into account all the forces described in section 2. Here we present our choices and their justifications.

3.1 Numerical integration of the equation of motion : Runge - Kutta

Our solution is the most straightforward: we consider the Solar System Barycenter frame to be inertial, and calculate the forces exerted on the probe in this frame. This gives us the equations of motion, which we solve numerically through a Runge-Kutta method. There are several other methods, for example a perturbative approach of the Keplerian problem. But we consider some non-standard forces for which the Lie developments are not known. Hence we favor the equations of motion as it is the simplest representation. Still, we had to answer several questions of computational efficiency.

3.2 Representing time

The first thing is to represent time efficiently. To do that, we use the Julian day [22]. This choice, common both in astronomy and in software development, allows for calculating numerically the time between two events easily. Also it makes Lorentz transformations simple.

3.3 Computing efficiently the position of the planets

Since the Newtonian gravitational field depends on the positions of the sun and the planets, the next thing is to find an algorithmically efficient way to know these positions at any given time. It would be incredibly inefficient to calculate them at each time step. It would be less but still highly inefficient to update them at each time step concurrently with the probe's position. Ultimately, the most efficient way is to calculate the positions at all times once, save them in a document, and read this document at each time step. This is essentially our strategy: we use the jplephem Python library from the Jet Propulsion Laboratory [23] which gives such a document, with a high precision on the positions.

3.4 Type of programming : object-oriented

Finally we had to find a way to compute the forces exerted on the probe. The naive approach is to calculate the accelerations from the formulas at each time step. But this makes the code much less modular and readable. We preferred to use object-oriented programming, hence we defined a class representing each kind of forces. We only have to instantiate one object from each class at the beginning of the algorithm and ask these objects for the forces at each time step. This does not make our algorithm any faster or memory-efficient, but it makes testing, debugging and usage much simpler.

3.5 Tests of precision

Indeed, since our objective is to discriminate between models of gravity that have the same {low speed & low mass} limit – that is the Newtonian gravity – we expect the differences in trajectories between models to be subtle. We must not bury these differences in the uncertainties and bias of our numerical integration. Hence we had to test the precision of our Runge-Kutta method.

To do so, we first computed the trajectories with a Newtonian potential and with a Yukawa potential. This gave us very similar trajectories that differed by only 15 m after 1 month. This is the precision our numerical integration needs to yield.

Then we computed the trajectory for a Keplerian problem both from the theoretical formula and from our library. We found that our numerical integration produces a drift of about 2 m per month. This is lower than the order of magnitude we aimed for, so our integration method is acceptable.

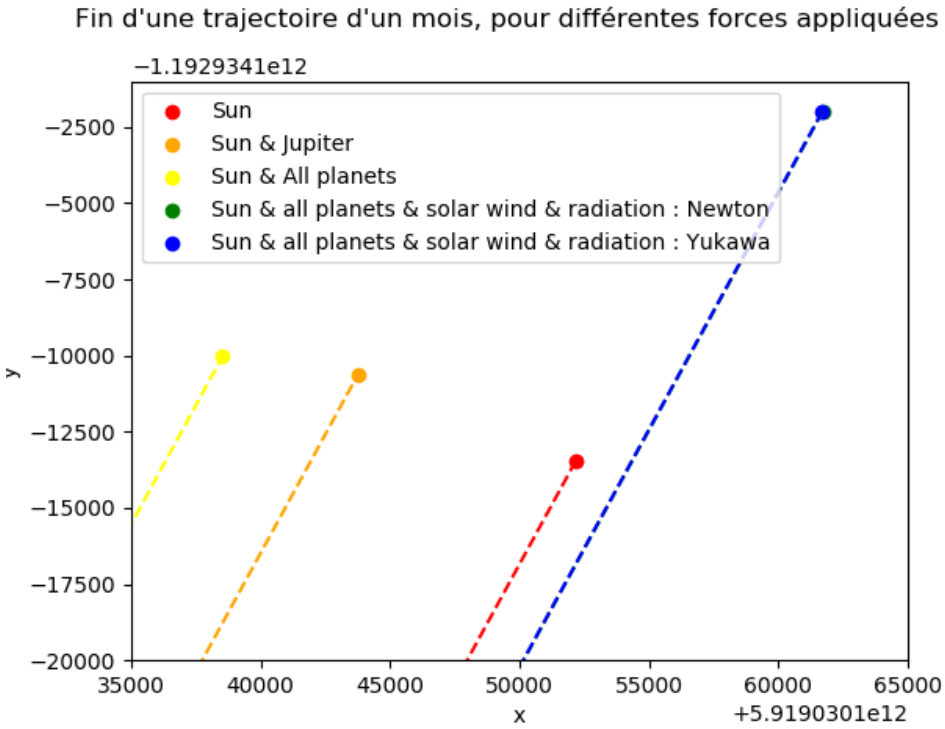

Figure 6: Position of the probe after 1 month of evolution, with the same initial position and velocity but under the influence of different forces.
In red only the influence of the Sun is considered. In orange we add the influence of Jupiter and in yellow that of all the other planets. In blue and green we also add the solar radiation pressure and the solar wind effects.
It appears that the Newton's and Yukawa's potentials give very similar trajectories. It also appears that none of the other forces considered is negligible.

4 Data analysis

As we have seen, Yukawa's potential is defined through two parameters α and λ, and the objective of our project is to find the values of those parameters that will yield trajectories that are significantly different from the trajectory in a Newtonian potential. We have spent the first semester developing the tools to simulate a trajectory. In this section, we outline how we use these tools to meet our objective.

4.1 Introduction of the χ^2 observable

In the actual mission, we would simulate the trajectory of the satellite for a given pair (α, λ) and then estimate the divergence of the simulated trajectory to the observed trajectory.

The first step would be to define the corrected observed trajectory y_{obs}, that is the trajectory the probe would have had in the absence of any non-gravitational effect. For that, we deduce from the observed trajectory x_{obs} the non-gravitational accelerations measured and we find the corrected trajectory by double time integration:

$$\vec{y_{obs}} = \vec{x_{obs}} - \iint \vec{x''_{NG}} dt_1 dt_2$$

But our corrected observed trajectory will have an uncertainty σ on each point. We study the origin and the evolution of σ with respect to time in Appendix B.

For the preliminary study that is this P3A, we have to simulate both the "model" and the "observation". The comparison between the "model" and the "observation" gives us the capacity of the accelerometer to discriminate between 2 models from their trajectory. Our "model" will be with the Newtonian potential and we will "observe" the Yukawa potentials. We represent the uncertainty σ by adding to the position, for each time step, a random variable following a normal law of variance $\sigma(t)$.

We can then quantify the difference between the "observed" trajectory and the "model" thanks to the χ^2 observable, which is defined as a comparison between the measured differences in the trajectories and the uncertainties on the measures :

$$\chi^2 = \sum_t \frac{|\vec{y_{obs}} - \vec{y_{model}}|^2}{\sigma(t)^2}$$

We define χ^2_{min} as the χ^2 between the model's trajectory and {the model's trajectory + an uncertainty σ}. The χ^2 becomes very useful then because a value of $\chi^2 - \chi^2_{min}$ larger than 6.7 means there is 95% certainty that the "model" and the "observation" truly are different trajectories.

4.2 Computing the χ^2 over an $\alpha - \lambda$ grid

Our objective is to find all the pairs (α, λ) that yield trajectories that would be statistically distinguishable from the Newtonian model. Hence we compute the χ^2 between a Newtonian model and a Yukawa model over a grid of pairs (α, λ).

We reasoned that we are looking for large χ^2, and that those correspond to trajectories that are very different from the Newtonian trajectory, hence to accelerations that are very different from the Newtonian acceleration. Since the radius of the orbits can be considered nearly constant over short simulation periods (less than a year), we can take the derivative of $||\vec{a_{Newton}} - \vec{a_{Yukawa}}||_2$ with respect to λ and find that $||\vec{a_{Newton}} - \vec{a_{Yukawa}}||_2$ is maximal when α is a little superior to r. This line of arguments gives us 2 useful information :

- The set of acceptable pairs (α, λ) will have the lowest α for $\lambda \approx r$. Since our mission will explore around $r = 40$ to 80 astronomical units, we should focus our numerical analysis on values of λ from 10^{11} to 10^{15} m.
- The shape of the set of acceptable pairs (α, λ) as drawn on a plane $(y, x) = (\alpha, \lambda)$ should look like a tongue with the lowest value at $\lambda \approx r$. This is what we observe on figure 3, for example for the planets for which the typical orbit radius is the astronomical unit (1 AU $\approx 10^{11}$m). Hence we can check if our code works properly by looking for this tongue-like shape.

Although we tried to optimise it algorithmically, the simulation of a trajectory is very time-consuming (1 hour for a simulation over 1 month). Since we have a large number of "observations" to make (a whole grid (α, λ)), we had to use a parallelized multi-processors approach. We used the Python library mpi4py [24] and about 2000 hours of computation on the school's processors. However, once the data for the trajectory is computed, the data analysis algorithm is fast and runs locally in a dozen of minutes.

4.3 Results

By simulating 4 trajectories per decade on α from $\alpha = 10^{-1}$ to 10^{-10} and 4 trajectories per decade on λ from $\lambda = 10^9$m to 10^{19}m, we find the results presented figure 7. The trajectories are that of a probe starting 1 AU further then Pluto with an initial speed of 0.05% c, during the month of January 2050.

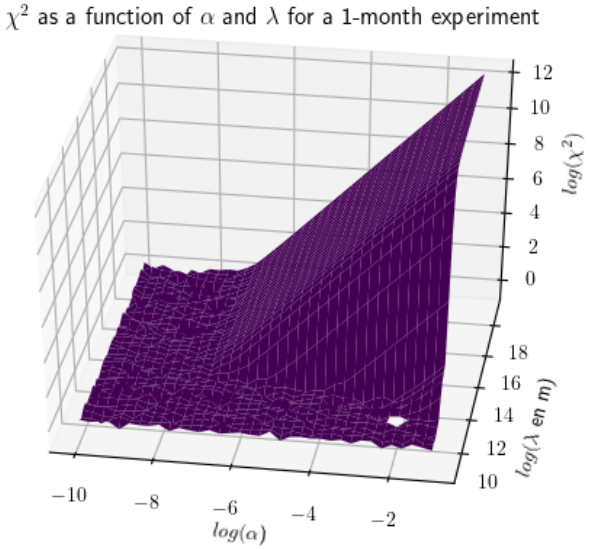

Figure 7: 3D plot of χ^2 as a function of α and λ

On the Z axis is the χ^2. We can make several interesting observations :

- There is a floor with $\log \chi^2 \approx -0.5$. Those are all the trajectories that are very close to the Newtonian model. The χ^2 does not reach 0 because its definition includes a random part that gives a minimum value very unlikely to be exceeded.
- The floor is uneven. Its fluctuations are also explained by the random part in the definition of the χ^2. This fluctuation of the floor informs us on the uncertainty we have on the χ^2. The fluctuation keeps the same size all over the grid (α, λ), but it disappears – when we plot $\log \chi^2$ – for large values of χ^2 because the log function flattens over large inputs.
- There is a point without a χ^2 at $\alpha = 10^{-2}$ and $\lambda = 10^{11}$. This is because it yielded a χ^2 that is lower than that of the Newtonian model. As counter-intuitive as it may seem, this is yet another effect of the random part in the χ^2's definition. This point should obviously not be interpreted as a model that is closer to the Newtonian model than the Newtonian model, but as a statistical quirk.

The value that determine whether the trajectory is statistically different from a Newtonian trajectory is $\log \chi^2 > 0.82$. We can therefore plot the set of pairs (α, λ) that yield trajectories that are significantly different from the Newtonian trajectory. This result is presented figure 8.

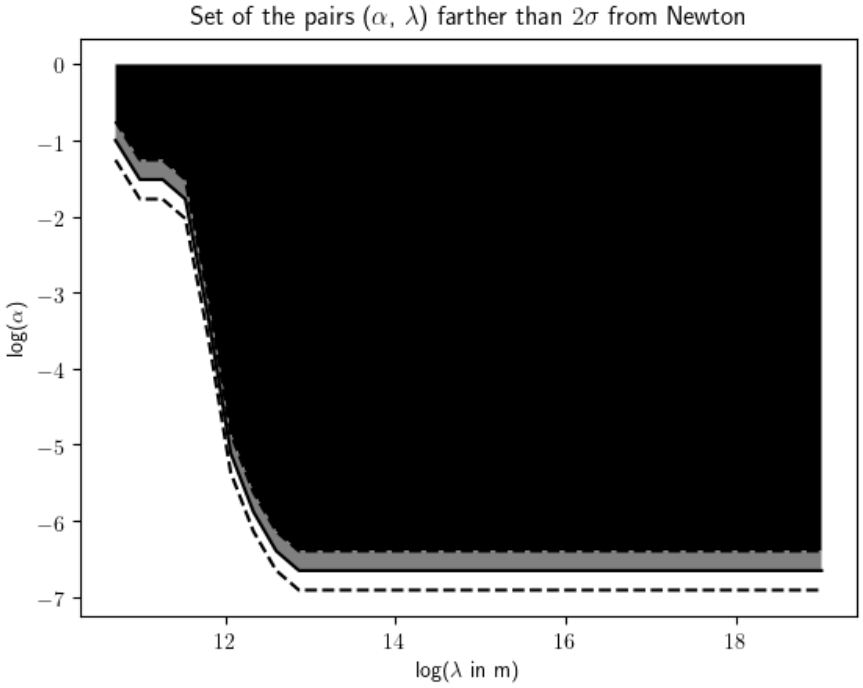

Figure 8: In black and grey the set of pairs (α, λ) that can be distinguished from the Newtonian model of gravity with the standard solar mass. The dotted black lines represent the uncertainties.

We notice that we do not find the shape expected in subsection 4.2 : when λ increases from 10^9m to 10^{13}m more and more α are accepted, and after $\lambda = 10^{13}$m there is a

saturation. Since the probe was positioned at 0.8 10^{13}m from the Sun, the rise at low λ fits quantitatively our prediction. However the saturation was not expected.

However, we understand this saturation: if we calculate the χ^2 only for the Newtonian model with the standard solar mass $M \approx 2\ 10^{30}$ kg, $||a_{\vec{Newton}} - a_{\vec{Yukawa}}||_2$ does rise from low λ to $\lambda = r$ then remains stationary.
But if we accept Newtonian models with an effective mass $M_{eff} = M \times (1 + \alpha)$, we find that $||a_{\vec{Newton}} - a_{\vec{Yukawa}}||_2$ reaches a maximum for $\lambda = r$ then decreases with λ^{-2}. This is the assumption done in figure 3, and this is why we expected a tongue shape in subsection 4.2.
However, our implementation only considers the Newtonian model with the standard solar mass. Hence, the discrepancy in shapes is not a numerical error. In figure 9 we extrapolate the limit we would have if we included models with modified solar mass into our calculation of χ^2 :

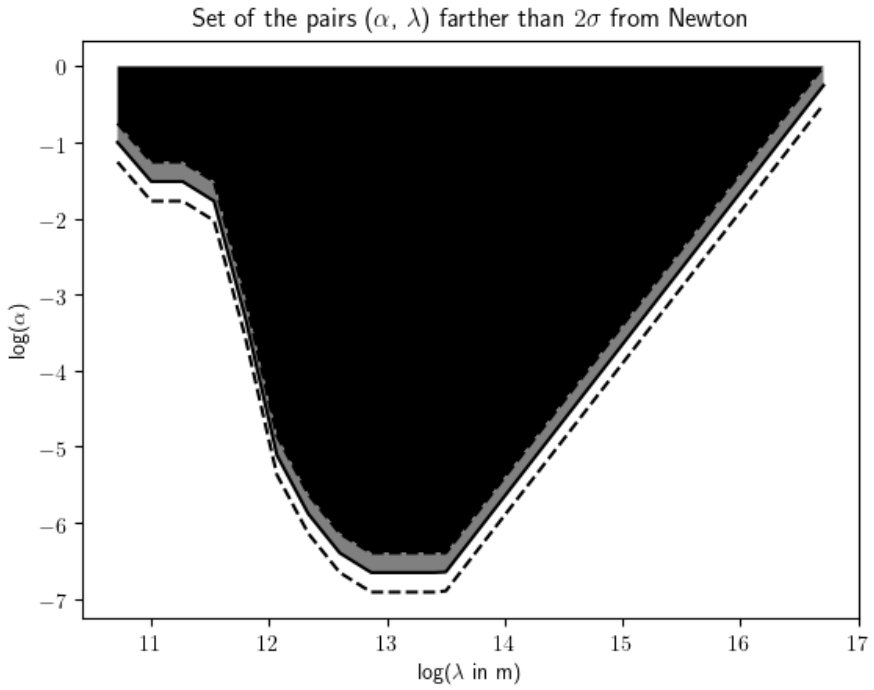

Figure 9: In black and grey the set of pairs (α, λ) that can be distinguished from Newtonian models of gravity with modified solar masses. The dotted black lines represent the uncertainties.

An interesting analysis we did not have the time nor the computing power to do is to increase the duration of the simulation from 1 month to 1 year to check if this allows for separating more pairs (α, λ).

Conclusion

The proposed Voyage 2050 mission's goal would be to investigate on several alternatives and corrections to general relativity that have been proposed in the literature to explain the observations that contradict general relativity. This P3A can be seen as a preliminary feasibility study that focuses on the tensor-scalar-vector theories, with the goal of finding the capability of ONERA's accelerometer to improve the current state of knowledge on these theories.

Our strategy consisted in developing a python library for simulating orbits in both Newtonian and Yukawa potential with sufficient precision and a limited computing power. For that we used a Runge-Kutta algorithm and an object-oriented coding paradigm. Then we used this library to simulate a Newtonian trajectory and several Yukawa trajectories in the outer solar system. Finally, we evaluate the statistical significance of the differences between those trajectories to find the pairs (α, λ) that the proposed Voyage 2050 mission would be able to study, with the current technologies of radars and accelerometers, thanks to the χ^2 observable.

We found that with the current technologies, the proposed mission would extend the boundaries on acceptable pairs (α, λ) up to the limit presented in figure 10 :

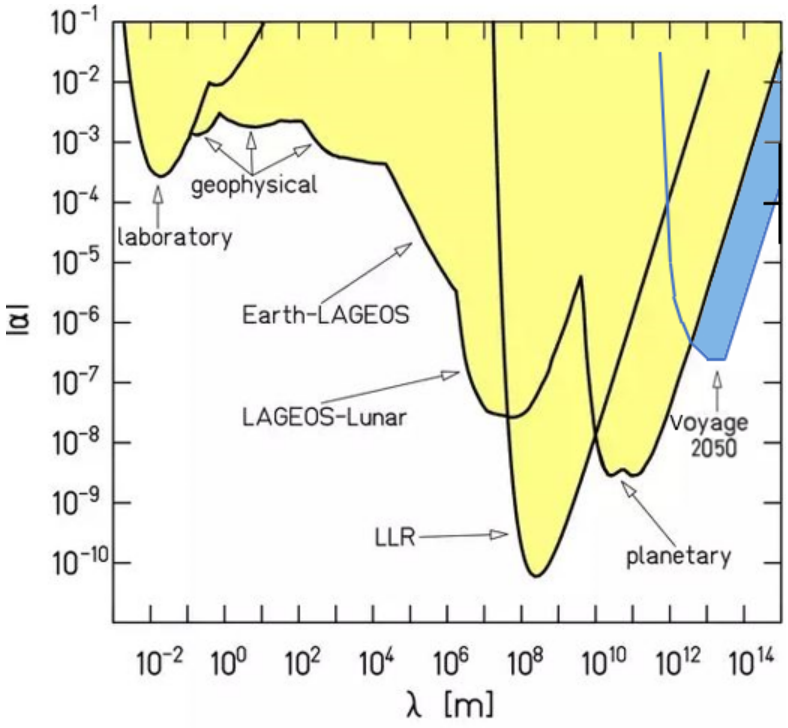

Figure 10: In yellow the boundaries on (α, λ) already obtained from past experiments [11], and in blue the boundaries that would be added by the proposed mission.

If we had more time, we could research the influence of the initial conditions on the ability of the accelerometer to discriminate between different values of α and λ, and the influence of the duration of the mission on the discrimination power.

Appendix A : Gravitational force exerted by the Kuiper belt

We decided to calculate the Kuiper belt's force by considering a homogeneous density torus with a circular cross-section. Afar from the torus, this model has has a semi-analytical solution which uses the complete elliptical integrals of the first and second kinds, two parametric integrals already saved as abacuses in the "Scipy" library in Python. This will help drastically decrease the time and computing power required in order to model the gravitational force of the belt.

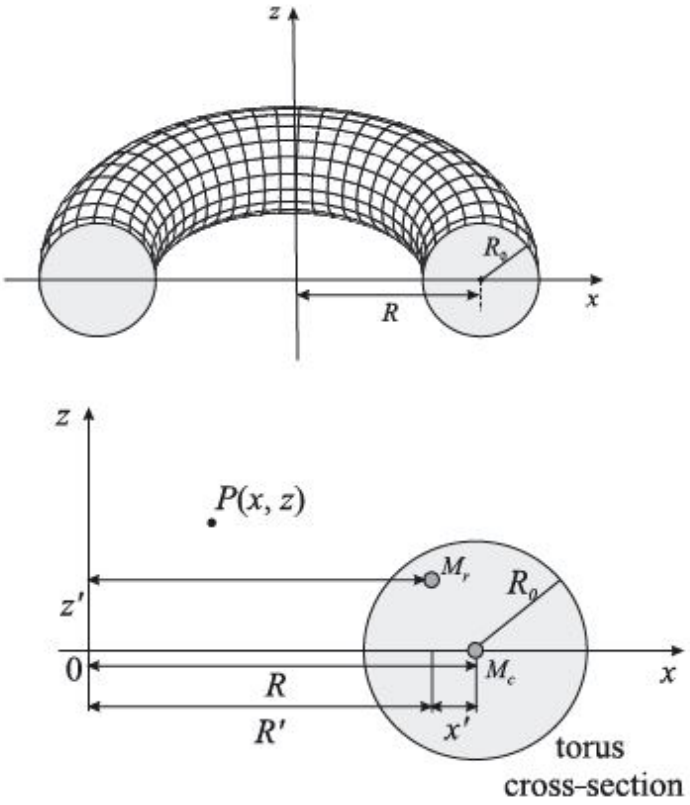

Figure 11: View of the torus model used for the Kuiper belt [14]

Newtonian gravitation

We start by calculating the potential of a circular ring. The ring is of mass M, of radius R and located in the plane z = 0 (see figure 11). We find its potential at an arbitrary point $P(x, z)$ by integrating the potentials created by infinitesimal elements of the ring and a few changes of variables :

$$\phi_c = -\frac{GM}{\pi R} \times \Phi_c(\tfrac{x}{R}, \tfrac{z}{R}) \text{ with } \Phi_c(\tfrac{x}{R}, \tfrac{z}{R}) = \sqrt{\tfrac{Rm}{x}} K(m)$$

Here $K(m) = \int_0^{\frac{\pi}{2}} \frac{d\beta}{\sqrt{1-m\sin\beta^2}}$ is the complete elliptical integral of the first kind with parameter $m = \frac{4xR}{(x+r)^2+z^2}$.

We now integrate this potential over all the rings that compose the torus to get the general expression of the potential. We use the notations R_0, x' et z' of figure 11 to parametrize the rings, then we introduce the normalized coordinates for the point $P(x,z)$: $\rho = \frac{x}{R}$ and $\zeta = \frac{z}{R}$, for the radius of the torus $r_0 = \frac{R_0}{R}$, and for the rings: $\eta' = \frac{x'}{R}$ and $\zeta' = \frac{z'}{R}$. We find the expression :

$$\phi_{torus}(\rho,\zeta) = -\frac{GM}{\pi^2 R r_0^2}\int_{-r_0}^{r_0}\int_{-\sqrt{r_0^2-\eta'^2}}^{\sqrt{r_0^2-\eta'^2}} \Phi_r(\rho,\zeta,\eta',\zeta')\,d\eta'\,d\zeta' \text{ with } \Phi_r = \sqrt{\frac{(q+\eta')m_r}{\rho}}K(m_r)$$

Here $K(m_r)$ is still the complete elliptical integral of the first kind, but now with parameter $m_r = \frac{4\rho(1+\eta')}{(1+\eta'+\rho)^2+(\zeta-\zeta')^2}$.

Finally, we take the Taylor development of Φ_r around $(\eta',\zeta') = (0,0)$ and find an approximation of the potential far from the torus, where this Taylor expansion is valid:

$$\phi_{torus}(\rho,\zeta,r_0) \approx -\frac{GM}{\pi R}\Phi_c \times \left(1 - \frac{r_0^2}{16} + \frac{r_0^2}{16}S(\rho,\zeta)\right) \text{ with } S(\rho,\zeta) = \frac{\rho^2+\zeta^2-1}{(\rho+1)^2+\zeta^2}\frac{E(m)}{K(m)}$$

Here K is the once again the complete elliptical integral of the first kind, E is the complete elliptical integral of the second time, and both take the parameter $m = \frac{4xR}{(x+r)^2+z^2}$. To find this simplified expression, we used the 2 following differential equations between K and E to calculate the derivative of those functions [15] :

$$\begin{cases} \frac{dE(m)}{dm} = \frac{E(m)-K(m)}{m} \\ \frac{dK(m)}{dm} = \frac{E(m)}{m(1-m^2)} - \frac{K(m)}{m} \end{cases}$$

This expression ultimately gives the Newtonian gravitational field exerted by the Kuiper belt by taking the gradient of the potential : $\vec{g} = -\vec{\nabla}\Phi_{torus}$. We simply have to perform the change of frame from the solar system's reference frame (in which we compute the trajectories) to the ecliptic plane's frame (in which the Kuiper belt does have z = 0).

Yukawa gravitation

The preceding method can be followed for a Yukawa potential, but with much less success because the definitions of K and E need to include an exponential term. Hence we loose the 2 differential equations between the 2 functions, and Φ_{torus}'s expression contains many terms, with first and second derivatives of K. Hence we had to create and use our own abacuses for K, $\frac{dK}{dm}$ and $\frac{d^2K}{dm^2}$.

Appendix B : Uncertainties from the mission's instruments

The Voyage 2050 mission is centered around 2 instruments. The first one is the radar that determines the position of the probe at all times. We consider a radar with the current technological standards, with an inherent uncertainty of about 1m [25] that is due both to the Earth's atmosphere and to the imprecision on the radar's pointing direction.

The second one is the accelerometer that measures the non-gravitational accelerations felt by the probe. We consider the accelerometer technology that ONERA embarked with success on the GOCE mission [11]. It works with a proof mass inside an cage. The cage carries electrodes which allow for measuring the mass' acceleration by capacitive sensing. But this kind of electrostatic sensing has an inherent bias that increases with time, hence it only allows for the measurement of relative accelerations. To overcome this issue, the cage rotates regularly by 180° around one of its axes. This is sufficient to cut the bias [26]. Overall, the accelerometer yields an accuracy on the absolute acceleration of 10^{-12} m.s^{-2}.

Hence, we have an uncertainty on the position measured at the present time t by the radar, an uncertainty on the initial speed of the probe, and an uncertainty on the non-gravitational accelerations measured at all past times t' by the accelerometer.

To model these uncertainties, we discretize the time with a step Δt, and assume that both the radar and the accelerometer do a measurement at each time step n. We model each measure by a random variable. At time $n\Delta t$, G_n is the gravitational acceleration, A_n is the non-gravitational acceleration, V_n is the speed, X_n is the observed position, and Y_n is the error on the corrected observed position. We have the following equations:

$$\begin{aligned} X_n &= X_0 + n\Delta t V_0 + \textstyle\sum_{i=1}^{n}(n-i+\frac{1}{2})\Delta t^2 G_i + \sum_{i=1}^{n}(n-i+\frac{1}{2})\Delta t^2 A_i \\ Y_n &= Y_0 + n\Delta t V_0 + \textstyle\sum_{i=1}^{n}(n-i+\frac{1}{2})\Delta t^2 G_i \end{aligned}$$

Since $Y_0 = X_0$ we find $Y_n = X_n - \sum_{i=1}^{n}(n-i+\frac{1}{2})\Delta t^2 A_i$. From now on, we denote with tildes the errors on each measurement (for example $Y_n = \bar{Y_n} + \tilde{Y_n}$). Then only the tilded terms are random variables. Hence we find $\tilde{Y_n} = \tilde{X_n} - \sum_{i=1}^{n}(n-i+\frac{1}{2})\Delta t^2 \tilde{A_i}$.

The variance of each of those variable is the standard deviation on the measurement. We assume that each $\tilde{A_n}$ has a variance ΔA and that each $\tilde{X_n}$ has a variance ΔX. We also assume that all these variable are independent, and follow a normal distribution. Hence we find that $\tilde{Y_n}$ follow a normal distribution as well, with standard deviation :

$$\begin{aligned} \Delta Y_n^2 &= \Delta X^2 + \textstyle\sum_{i=1}^{n}((n-i+\frac{1}{2})\Delta t^2)^2 \Delta A^2 \\ &= \Delta X^2 + \tfrac{n(4n^2-1)}{12}\Delta t^4 \Delta A^2 \end{aligned}$$

This gives us the uncertainty on each point of our "observations", and allow us to compute the χ^2 observable.

Bibliography

[1] Wikipedia article on Einstein's Field Equations. Last consulted on 10/12/2019

[2] Wikipedia article on the galaxies' rotation curves. Last consulted on 10/12/2019

[3] Website on which figure 1 was found. Last consulted on 10/12/2019

[4] Web page explaining how F. Zwicky postulated the existence of unseen matter. Last consulted on 10/12/2019

[5] Wikipedia article on dark matter. Last consulted on 10/12/2019

[6] Wikipedia article on the Weakly Interacting Massive Particles. Last consulted on 10/12/2019

[7] Wikipedia article on dark energy. Last consulted on 10/12/2019

[8] Website on which figure 2 was found. Last consulted on 10/12/2019

[9] Wikipedia article on tensor-scalar-vector theories. Last consulted on 10/12/2019

[10] Wikipedia article on the Chameleon Particle Theory. Last consulted on 10/12/2019

[11] J. Berge, F. Liorzou, B. Christophe. Testing gravity beyond the standard model: status of GAP, an electrostatic accelerometer for interplanetary fundamental physics. The 40th COSPAR Scientific Assembly (COSPAR 2014), Aug 2014, MOSCOU, Russia.

[12] Wikipedia article on the equivalence principle. Last consulted on 10/12/2019

[13] E. Yu. Bannikova, V. G. Vakulik, A. V. Sergeev, N-body simulation of a clumpy torus: application to active galactic nuclei. Mon. Rot. R. Astron. Soc. 424, 2012

[14] E. Yu. Bannikova, V. G. Vakulik, V. M. Shulga, Gravitational potential of a homogeneous circular torus : a new approach. Mon. Rot. R. Astron. Soc. 411, 2011

[15] Wikipedia article on the elliptical integrals. Last consulted 27/02/2020

[16] Satellite Orbits, O. Montenbruck & E. Gill, Springer, First Edition, 2000

[17] Wikipedia article on the solar winds. Last consulted on 10/12/2019

[18] Online article about the solar winds. Last consulted on 10/12/2019

[19] Online article about the solar winds. Last consulted on 10/12/2019

[20] Support for Temporally Varying Behavior of the Pioneer Anomaly from the Extended Pioneer 10 and 11 Doppler Data Sets, S. G. Turyshev & V. T. Thot & J. Ellis & C. B. Markwardt, Physical Review Letters, 107, 2011

[21] French Wikipedia article on interstellar dust. Last consulted 20/12/2019

[22] Wikipedia article on the Julian day. Last consulted 19/12/2019

[23] Repository and documentation of the jplephem Python library

[24] Repository and documentation of the mpi4py Python library

[25] Testing long-distance modifications of gravity to 100 astronomical units, B. Buscaino & D. DeBra & P. W. Graham & G. Gratta & T. D. Wiser, Physical Review D, 92, 2015

[26] Unbiased acceleration measurements with an electrostatic accelerometer on a rotating platform, B. Lenoir & B. Christophe & S. Reynaud, Advances in Space Research, 51, 2012